

Artificial receptors for the electrochemical detection of bacterial flagellar filaments from *Proteus mirabilis*

*M. Azizur R. Khan*¹, *A. Rita Aires Cardoso*², *M. Goreti F. Sales*^{*2}, *Susana Merino*³, *Juan M. Tomás*³, *F. Xavier Rius*¹, *Jordi Riu*¹

¹Universitat Rovira i Virgili, Department of Analytical and Organic Chemistry,
C/ Marcel·lí Domingo s/n, 43007 Tarragona, Spain.

²BioMark/ISEP, School of Engineering of the Polytechnic Institute of Porto,
Porto, Portugal.

³Universitat de Barcelona, Department of Microbiology,
Barcelona, Spain.

<https://doi.org/10.1016/j.snb.2017.01.018>

* Corresponding author at: BioMark, Sensor Research, Instituto Superior de Engenharia do Porto,
Rua Dr. António Bernardino de Almeida 431, 4200-072 Porto, Portugal. E-mail address:
mgf@isep.ipp.pt

Abstract

In this paper for the first time we successfully detect bacterial flagellar filaments from *Proteus mirabilis* using molecularly imprinted artificial receptors. These receptors acted as a sensing layer of the biosensors, assembled by imprinting flagellar proteins onto a polymeric backbone of electropolymerized phenol. In short, flagellar filaments were absorbed onto a carbon support, phenol was electropolymerized around it through the carbon conductive matrix to create the protein molecular molds, and finally the flagellar proteins were removed by enzymatic and electrochemical action. Each removed flagellar protein gave rise to an imprinted site with eventual rebinding ability.

Electrical impedance spectroscopy (EIS) and square wave voltammetry (SWV) were employed to measure the interaction of flagellar filaments with the sensing layer assembled on commercial screen-printed electrodes, providing low detection limits, high precision and selectivity toward the targeted protein. The detection limit was 0.7 ng/mL by EIS and 0.9 ng/mL by SWV. The artificial receptors were further assembled on home-made paper-printed electrodes, with the three-electrode system printed on a paper substrate, offering the possibility of detecting flagellar filaments at as low as 0.6 ng/mL with a disposable and cost-effective portable device.

To the best of our knowledge this is the first sensing device where molecularly imprinted artificial receptors are tailored on home-made electrode based on paper substrates with three electrodes assembled together, which is a suitable approach for the fabrication of easy and cost-effective tailored electrodes.

Keywords: Molecularly imprinted polymers; Artificial receptors; Flagellar filaments; *Proteus mirabilis*; Screen-printed electrodes; Paper-printed electrodes; Electropolymerization; Disposable device.

1. Introduction

Bacteria are present in a variety of sources including food, water, animals, the environment and the human body. The detection of pathogenic bacteria is extremely important for health and safety reasons. Detecting bacteria with biosensors has been proposed using a variety of analytical detection techniques such as reflectometric interference spectroscopy [1], fluorescence [2], quartz crystal microbalance [3,4], electrochemical methods [5–8] or surface plasmon resonance (SPR) [9]. Work has recently focused on detecting specific bacterial markers, referred to as pathogen-associated molecular patterns, rather than on whole cell detection [10,11]. These markers include, but are not limited to, intercellular entities such as DNA [12,13] or extracellular components like lipopolysaccharides (LPS) or flagellar filaments [14,15].

Flagellar filaments are located on the outer surface of bacteria and can act as markers for detecting and/or identifying bacteria. In this regard, clinical studies have revealed the significant role of flagellar filaments in the characterization and affiliation of anaerobic bacteria [16]. Also, in natural aquatic environments flagellar filaments can be used as biomarkers [17,18], and in mechanistic studies they can be used to observe the motility behavior of bacteria.

Different strategies exist for staining and detecting bacterial flagellar filaments, including the fuchsin-tannic acid method [16] and subsequent modifications [19,20], and silver staining methods [16]. These approaches are satisfactory but involve complicated protocols. In addition, each method has limitations such as time, unstable reagents and fixation-induced alterations. Therefore there are still key issues that need to be considered in the development of rapid methods for the detection of bacteria and/or flagellar filaments with acceptable levels of cost, simplicity, training, and accuracy [21]. Alternative methods for detecting bacterial flagellar

filaments on-site would facilitate the characterization/quantification of clinical and environmental bacterial isolates.

This paper describes a novel, rapid and label-free method for the detection of bacterial flagellar filaments. It uses an artificial receptor as a biorecognition element, as this may offer a promising alternative to antibodies and other biological receptors currently used in biosensors. The most generic and cost-effective technique for preparing synthetic receptors is molecular imprinting. This combines high affinity and specificity with robustness and low manufacturing costs to generate molecularly imprinted polymers (MIPs), also known as artificial receptors [22]. As far as we know, several strategies have been reported for the detection of bacterial flagellar filaments, but none of them make use of molecularly imprinted polymers. The fabrication of MIP-based receptors for small molecules is quite straightforward and these receptors have been successfully used in extraction, separation, binding, detection, enzyme-like catalysis and drug delivery. However, MIP-based receptor preparation for large molecules such as proteins is rather difficult although promising [22–24]. The preparation of MIP-based materials for large templates such as flagellar filaments is therefore even more difficult.

In molecular imprinting, monomeric structures are polymerized to form a well-organized structure surrounding the target (herein, the flagellar filaments) in a complex polymeric network via covalent and/or non-covalent interactions. Customized specific binding sites that conserve the size, shape and orientation of the target (key-lock approaches) are created by the subsequent removal of the target from the polymeric network. The binding cavities generated are selectively used as recognition sites for the target, like in natural antibody and antigenic interactions. Hence the materials can be termed artificial or man-made antibodies for capturing specific target analytes [25,26].

In this paper we detect flagellar filaments from *Proteus mirabilis* (FFPM) as proof of concept for the detection of flagellar filaments using artificial antibodies as a biorecognition element. *Proteus mirabilis* is a widely distributed bacterium in soils and water and has the ability to produce high levels of urease. It may be responsible for urinary tract infections with serious complications including cystitis, acute pyelonephritis, fever, bacteremia, and death [27]. To the best of our knowledge, there are no previous MIP-based biosensors for the detection of flagellar filaments. We are therefore able to create a MIP using flagellar filaments as the template for the first time, and MIP-based biosensors are used for the impedimetric (EIS) and square wave voltammetric (SWV) detection of flagellar filaments from *Proteus mirabilis* with high selectivity and precision. Furthermore, the biorecognition element is assembled on home-made paper substrates, creating, as far as we know, the first device based on molecularly imprinted artificial receptors built on paper substrates with three electrodes assembled together, thereby helping to the fabrication of simple cost-effective tailored electrodes.

2. Experimental section

2.1 Apparatus

The electrochemical measurements were made with a potentiostat/galvanostat from Metrohm Autolab and a PGSTAT302N (Utrecht, The Netherlands), equipped with an FRA module and controlled by Nova software. The single-walled carbon nanotubes screen-printed electrodes (SWCNTs-SPEs) were purchased from DropSens (Oviedo, Spain), and were composed of a working electrode made of carboxylated SWCNTs, a counter electrode made of carbon and a reference electrode and electrical contacts made of silver. The diameter of the working electrode was 3.80 mm. The SWCNTs-SPEs were connected to a portable switch box, also from DropSens (DRP-DSC), allowing their interface with the potentiostat/galvanostat.

As an alternative to commercial SWCNTs-SPEs, homemade paper-based carbon-printed electrodes (identified herein as HP C-PEs) were made in our laboratory by coating a filter paper with paraffin wax to make it hydrophobic and manually printing the three electrodes with carbon ink (Creative Materials, USA). One of the three electrodes was coated with Ag/AgCl (Creative Material, USA) to make the reference electrode. The final system was covered with a plastic mask which was connected to a portable switch box, also from DropSens (DRP-DSC), allowing its interface with the potentiostat/galvanostat.

Raman measurements were performed using a Thermo Scientific DXR Raman spectrometer with confocal microscopy (Waltham, USA), with a 10 mW 532 nm excitation laser.

2.2 Reagents

All chemicals were of analytical grade and the water used throughout was de-ionized or ultrapure Milli-Q laboratory grade. The potassium hexacyanoferrate III, potassium hexacyanoferrate II trihydrate, and sodium acetate anhydrous were obtained from Riedel-deHäen; proteinase K from Fluka 99%; 2-(*N*-morpholino)ethanesulphonic acid monohydrate 98% (MES) from Alfa Aesar; phenol, bovine serum albumin (BSA), and protein A (PA) from *Staphylococcus aureus* was from Sigma Aldrich, and potassium chloride (KCl) from Merck.

2.3 Flagella from *Proteus mirabilis*

Proteus mirabilis was grown in Luria Broth at 37°C for flagellar filaments purification. Cells were collected by centrifugation at $5000 \times g$, and suspended in 100 mM Tris (pH = 7.8) buffer. Flagellar filaments were removed from the cells by shearing in a vortex with a glass bar for 3-4 min, and then passing repetitively (minimum six times) through a syringe. Cells were removed by centrifugation at $8000 \times g$ for 30 min, and the supernatant centrifuged at $18000 \times$

g for 20 min. From the remaining supernatant, the filaments were pelleted by ultracentrifugation at $100000 \times g$ for 60 min, and resuspended in 100 mM Tris (pH = 7.8) plus 2 mM EDTA buffer. Such filaments enriched fraction was purified in a cesium chloride gradient by ultracentrifugation at $60000 \times g$ for 48 h. The band containing the flagellar filaments were collected and the cesium chloride removed by extensive dialysis against the same buffer (100 mM Tris, 2 mM EDTA). The purity of flagellar filaments was assessed by SDS-PAGE (sodium dodecyl sulfate polyacrylamide gel electrophoresis) and Coomassie blue staining (Figure S1 Supplementary Information). The monomeric flagellin concentration was determined by densitometry of the 39 KDa band and comparison with standard proteins with similar molecular weight and known amount. The integrity of the purified flagellar filaments were checked by transmission electron microscopy (TEM) (Figure S2 Supplementary Information). Purified flagellar filaments were diluted ($0.01 \mu\text{g}/\text{mL}$), placed on Formvar-coated grids and negative stained with a 2% solution of uranyl acetate pH 4.1. Preparations were observed on a Jeol JEM 1010 transmission electron microscope and electron micrograph show flagellar filaments with little variable length.

Flagellar filaments from *Escherichia coli* DH5- α (FFED) and from *Aeromonas* AH-3 (FFAA) were obtained in a similar way as FFPM are obtained. These flagellar filaments were used in the selectivity studies.

2.4 Solutions

Stock solutions of $1000 \mu\text{g}/\text{mL}$ of flagellar filaments from *Proteus mirabilis* (FFPM) were prepared in TRIS buffer ($6.66 \times 10^{-4} \text{ mol}/\text{L}$, pH 7.8) and stored at -20°C . Standards were obtained by accurate dilution of the previous solution in MES buffer ($1.0 \times 10^{-2} \text{ mol}/\text{L}$, pH 5.0, KCl 0.1 mol/L), depending on the applications. Electrochemical assays were performed with $5.0 \times 10^{-3} \text{ mol}/\text{L}$ $[\text{Fe}(\text{CN})_6]^{3-}$ and $5.0 \times 10^{-3} \text{ mol}/\text{L}$ $[\text{Fe}(\text{CN})_6]^{4-}$, prepared in MES buffer. The

selectivity study was performed using the competitive method in MES buffer using globular proteins BSA (0.85 $\mu\text{g/mL}$) and PA (0.51 $\mu\text{g/mL}$), and flagellar filaments FFED (1.03 $\mu\text{g/mL}$) and FFAA (1.27 $\mu\text{g/mL}$).

2.5 Electrochemical synthesis of imprinted and non-imprinted films

Prior to electropolymerization, the SWCNTs-SPEs were cleaned using chronoamperometry (+1.7 V for 60 s, with KCl 0.1 mol/L) and stabilized electrochemically with MES buffer by cyclic voltammetry (CV, potential from -0.2 to $+0.8$ V, 10 cycles, and scan-rate of 50 mV/s). In the case of the HP C-PEs, the electrodes were cleaned by CV (potential from -2.0 to $+2.0$ V, 40 cycles, and scan-rate of 100 mV/s in KCl 0.1 mol/L), and stabilized electrochemically in the same way as for SWCNTs-SPEs.

For imprinting the flagellar filaments on the SWCNTs-SPE, 10 μL of 100 $\mu\text{g/mL}$ FFPM solution prepared in MES buffer was placed over the working electrode area for 30 min at room temperature, and then gently washed off with Milli-Q water. 75 μL of phenol solution (3.55×10^{-3} mol/L prepared in acetate buffer 1.0×10^{-2} mol/L pH 5.0) was deposited onto the SWCNTs-SPE to cover the three-electrodes for ~ 10 s, and polymerization was performed by CV between -0.2 and $+0.8$ V (scan-rate of 50 mV/s, 15 CV cycles was found to be optimal). For the HP C-PEs, the procedure was the same as for the SWCNTs-SPEs, but the potential range of electropolymerization was set from -0.2 to $+1.2$ V.

The resulting polymeric film (either in SWCNTs-SPEs or in HP C-PEs) was thoroughly washed with deionized water and incubated with proteinase K (500 $\mu\text{g/mL}$ in PBS pH 7.4) for 2.5 h at room temperature. The surface was then thoroughly washed with Milli-Q water and subjected to subsequent electrochemical cleaning by 25 CV cycles in MES buffer (potential

range -0.2 to $+0.8$ V, scan rate 50 mV/s). The synthesis of the artificial receptors based on molecularly imprinted polymers (MIPs) is schematically presented in [Figure 1](#).

—Please insert Figure 1 here

In parallel, non-imprinted polymers (NIPs) were synthesized in a similar way but without the presence of FFPM. All the steps involved in the fabrication of the imprinted and non-imprinted polymers were followed by CV, EIS and SWV.

2.6 Qualitative characterization of the films

Qualitative analyses of the various stages of the assembly of the biorecognition film were performed directly on the SWCNTs-SPE by Raman spectroscopy, without any treatment of MIP and NIP films. The spectra were collected by 1 mW laser power at sample, 10 minutes photo bleaching time, and 50 μm slit aperture.

2.7 Binding isotherm

The rebinding properties of MIP- and NIP-based biosensors on SWCNTs-SPEs were measured by calculating an approximate value (see Supplementary Information) of the apparent dissociation constant (K_D) using EIS and SWV assays. FFPM standards ranging from ng/mL to $\mu\text{g/mL}$ concentrations were prepared in MES buffer, and each standard was incubated 50 min before adding the redox probes for subsequent EIS and SWV measurements.

A Langmuir isotherm model ([Eq. \(1\)](#)) was applied to the experimental data, as described in Moreira *et al.* 2013 [28]. In this equation, R_{ct} is the normalized charge transfer density ($\text{k}\Omega/\text{cm}^2$), S is the concentration of FFPM (in M), R_{ct}^{max} is the maximum charge transfer density

observed ($k\Omega/cm^2$) and K_D is the concentration (in $\mu g/mL$) of flagellar filaments required to give half of the maximum response produced by the device. K_D and R_{ct}^{max} were calculated from fitting the experimental data to the model in Eq. (1). Concomitantly, the Langmuir isotherm model was applied to the SWV data, in a similar way to that described for EIS.

$$R_{ct} = \frac{R_{ct}^{max}}{1 + K_D/[S]} \quad (1)$$

2.8 Electrochemical assays

The redox probes in all CV and EIS measurements were 5.0 mmol/L $[Fe(CN)_6]^{3-}$ and 5.0 mmol/L $[Fe(CN)_6]^{4-}$ prepared in MES buffer at pH 5.0. In the CV assays the potential range was from -0.5 to $+0.7$ V, at 50 mV/s. In the EIS, an open circuit potential was set using a sinusoidal potential perturbation of 0.01 V amplitude and 50 logarithmically distributed frequency values over a frequency range of 0.01 Hz to 100 kHz. In the SWV assays the potential range was from -0.4 to $+0.6$ V.

Calibrations were performed by EIS and SWV measurements for FFPM in the range from 0.12 nM to 1.22 μM . At each concentration level, 10 μL of FFPM in MES buffer was exposed to the imprinted sensor surface for 50 min at room temperature. The values of precision corresponded to the standard deviation of triplicate experiments of different electrodes. Selectivity studies were conducted by using BSA, PA from *Staphylococcus aureus* and flagellar filaments FFED and FFAA in MES buffer at pH 5.0. Real sample analysis was done by spiking FFPM in tap water (four times diluted in MES buffer) using the home-made paper-based (HP C-PE) electrode.

3. Results and discussion

3.1. Polymer growth

The polymeric film acted as the biorecognition element of the biosensor and was generated by electropolymerization. This was achieved by CV consecutive cycling (up to 15 cycles) on a phenol solution placed over the SPEs modified with a layer of flagellar proteins (in the case of MIP-based devices) or over bare SPEs (in the case of NIP-based devices), for both commercial SWCNTs-SPEs (Figures 2A and 2B) and HP C-PEs (Figures 2C and 2D).

The cyclic voltammograms obtained for SWCNTs-SPEs are displayed in Figure 2A. In brief, the anodic current peak in the direct scan corresponding to the oxidation of phenol is observed at +0.5 V for MIP films with low intensity of current, whereas NIPs showed a maximum peak position at around +0.6 V with higher intensity of current. The presence of the protein on the MIP layer was responsible for the lower currents obtained, while the higher potential of the NIP layer evidenced the slow electron transfer kinetics of the reaction, revealing changes in the rate of mass transport to the electrode surface. This is consistent with the fact that the oxidation of phenol occurred by irreversible direct electron transfer, accounting for the absence of the reduction peak on the reverse scan.

The anodic currents were reduced in the second scan leading to the production of polyphenol. The CV data evidenced the formation of a non-conductive and electro-inactive polymeric film at the electrode surface, hindering the direct electron transfer and/or diffusion of phenol molecules to the anode surface. This decrease in current was more intense in the NIP material (from 140 μA to 30 μA , from first to second scan) than in the MIP (from 100 μA to 60 μA). This was supported by the fact that the NIP electrode displayed higher currents at the beginning, meaning that a higher electrical stimulus was driving the NIP polymerization forward. As the growing polymer is a non-conductive material, the electrical current dropped more for thicker layers of polymeric film. Consistently, as the number of successive cycles

increased, the anodic peak current diminished, until a steady state was achieved (after 7 cycles for MIPs or 4 cycles in the case of NIPs).

—Please insert Figure 2 here

After concluding the polymerization stage, the electrical output of the MIP and NIP films was recorded using an iron redox probe. As can be seen in [Figure 2B](#), the resulting CV data showed a significant current decrease in both MIP and NIP films when compared to the clean SWCNTs-SPEs. This behavior also evidenced the existence of polymer at the electrode surface.

The same procedure was applied to the MIP-based home-made electrodes prepared herein. The results obtained are shown in [Figures 2C and 2D](#). Compared to the commercial SWCNTs electrodes, the background electrical signal of the HP C-PEs was smaller by about 14.9% (CV data in [Figures 2B and 2D](#)). This was due to the smaller physical area of the working electrode made in the laboratory; the SWCNTs-SPEs were 45 mm² and the HP C-PEs were 38 mm². Apart from this, a similar behavior to that of the SWCNTs electrodes was observed. The presence of the flagellar proteins on the clean HP C-PE reduced its intrinsic anodic current and shifted the peak potential of the monomer close to 0.8 V ([Figure 2C](#)). In addition, the consecutive CVs involved in the polymerization process promoted significant additional current decay, as expected ([Figures 2C and 2D](#)).

3.2 Template removal

The follow-up of the protein template exit from the polymeric material was made by EIS and SWV, measured before and after FFPM removal ([Figure 3](#); clean SWCNTs-SPEs were also included for control purposes). The EIS data fitted the Randles equivalent circuit. In this,

the semicircles (observed at high frequency range) indicated a charge-transfer controlled process. The diameter of this semicircle equaled the charge-transfer resistance, R_{ct} , which controlled the electron-transfer kinetics of the redox-probe at the electrode interface [29]. The linear behavior was given at the low frequency range and revealed a diffusion-controlled mass-transfer process [30], measured by the Warburg element (W). Overall, the electrical circuit in EIS consisted of a resistor element (solution resistance, R_s) in series with one parallel circuit comprising a charge transfer resistance, R_{ct} , with a Warburg element (W) and a double layer capacitance, C_{dl} (inset, [Figures 3A, 3B](#)) [31–33].

—Please insert Figure 3 here

After electropolymerization, MIPs showed higher EIS-based R_{ct} than NIPs, though the polymerization was lower in MIPs than NIPs ([Figures 3A and 3B](#)). This is consistent with the fact that both FFPM and polyphenol are coating the electrodes in MIP films, while only polyphenol is present in NIP-based electrodes. In addition, this behaviour is the ultimate indication that the presence of FFPM alone increases the charge transfer resistance of the electrodes.

FFPM removal was achieved by the proteolytic action of proteinase K. The peptide fragments generated by this process were then removed from the surface by subsequent chemical (washing) and electrochemical cleaning (consecutive CVs). As expected, the ultimate result of this process generated a decrease in the charge transfer resistance, R_{ct} ([Figures 3A and 3B](#)). This decrease correlated well with the protein exit from the sensing layer, as the previous addition of FFPM to the electrode surface promoted a R_{ct} increase. In addition, as the NIP films also showed a small R_{ct} decrease (to a lesser degree than the MIP ones), a small part of the R_{ct}

reduction observed in the NIP film may be evidencing the exit of small polymer fragments and unreacted species that were not firmly attached to the electrode surface.

SWV data are shown in [Figures 3C and 3D](#) and were also consistent with the behaviour observed in EIS. The electrical current generated by an iron redox probe on the MIP film holding the protein was much lower than on the NIP film, thereby confirming the presence of the protein within the polymer. In turn, the subsequent removal of the protein led to a significant increase in current in the MIP film; the NIP film current increased by only a small amount and remained with lower currents than the MIP material.

The surface modification of HP C-PE-based MIPs was also followed by SWV, showing similar behaviour to the MIP films relying on SWCNTs-SPEs. The corresponding data have been added as supplementary material ([Figure S3](#)). Overall, the above data were powerful evidence of the successful imprinting procedures, whereby the intended rebinding cavities were generated. In parallel to the electrical readings, the chemical modifications occurring at the electrode surface were also followed up by Raman spectroscopy.

3.3 Raman spectroscopy follow-up

The electropolymerized films of phenol are produced by *ortho*- or *para*- coupling of phenoxy radicals generated by oxidation of the phenolate anion. The necessary electrical conditions were established by CV, whereby the minimum voltage to promote the phenol oxidation on the underlying substrate was identified. Subsequent reactions to produce the intended polyphenol polymers were promoted by consecutive CV recordings [34,35]. The resulting polymers were directly observed by Raman analysis with confocal microscopy, in order to have some qualitative data on the newly formed chemical structures.

The spectra obtained are presented in [Figure S4](#) (Supplementary Information). As the background support in all electrodes is carbon, the typical G and D and 2D bands appeared in the spectra.

Regarding the D and G bands, the intensity ratio I_D/I_G of the clean SWCNTs-SPE was 1.078, whereas the ratios for the MIP and NIP films were 1.069 and 1.068 respectively. Although the ratio values were quite similar, the MIP and NIP peaks have a broader shape when compared to the clean SWCNTs-SPE control materials, indicating surface coverage by carbon polymeric material. As expected, the polymeric-based devices (MIPs and NIPs) showed similar behavior in terms of broader peak shape, which is consistent with the fact that the chemical composition of these films was similar. Although the NIP films were expected to have a thicker film of polymeric material on top of the carbon background, in terms of intensity ratio this difference would not be reflected in the Raman data.

Greater differences between the control and polymeric materials (MIP and NIP) were observed in the 2D peaks. In general, the 2D peak intensity is assigned as an inverse relationship with the surface layer and/or coverage. The control SWCNTs material had a higher Raman intensity, which decreased after a polymeric film was created on top of it.

Overall, the Raman spectra confirmed the chemical differences between the control and the polymeric materials, thereby corroborating the presence of the polyphenol film on top of the carbon background, and that the presence of FFPM at the imprinting stage had no effect on the final sensing layer. In addition, this similarity between the MIP and NIP films also confirmed that the action of proteinase K had no effect during the template removal.

3.4 Main analytical features

In [Figure 3A](#), the charge transfer resistance (R_{ct}) after template removal is a little bit higher than the corresponding R_{ct} for MIPs in [Figure 4A](#). This is probably because MIPs in [Figure 3A](#) were synthesized in organic buffer (sodium acetate) without the presence of KCl salt, whereas the R_{ct} value in the case of MIPs (after template removal) in [Figure 4A](#) is slightly lower since MIPs were stabilized (before starting calibration) in MES buffer containing a high salt

concentration (KCl 0.1M). Probably the MES and salt environment may introduce some charges into the polymeric backbone which facilitate charge transfers from redox probes and hence the R_{ct} may differ. A similar behaviour was observed in the case of NIPs. Interestingly, SWV does not show significant differences of intensity of current values, which is probably due to the higher sensitivity of EIS compared to SWV.

The EIS and SWV responses of both the MIP and NIP sensors to increasing concentrations of FFPM are shown in Figure 4. The raw data for the MIP and NIP films are shown in Figures 4A and 4B for the EIS assays and in Figures 4D and 4E for the SWV. The corresponding calibration curves are shown in Figures 4C and 4F respectively.

In general, the NIP-based devices presented a negligible response in the presence of increasing concentrations of FFPM, in both the EIS and the SWV assays (Figures 4B and 4E). This confirmed the lack of affinity of the non-imprinted polyphenol receptor surface towards the target protein (and therefore its unimportant contribution to the performance of the final device). Thus the target FFPM protein displays lower non-specific binding affinity towards the polyphenol surface.

The MIP devices, however, showed very sensitive changes to increasing FFPM concentrations (Figures 4A and 4D). In the EIS data (Figure 4A), the semicircles became larger as the FFPM concentration increased. This was probably due to the increase in the thickness and passiveness of the MIP surface caused by the captured FFPM, which in turn hindered the electron transfer of negatively charged iron redox probe molecules at the surface. The average slope of this process was $0.27 \text{ decade}^{-1} \cdot (\mu\text{g/mL})^{-1}$ ($860 \Omega/\text{decade} \cdot (\mu\text{g/mL})^{-1}$ reverting the ratio of $R_{ct}/R_{o,ct}$ by multiplying by $R_{o,ct}$) for a linear range of over three orders of magnitude, from $0.01 \mu\text{g/mL}$ up to $60 \mu\text{g/mL}$ (Figure 4C). The detection limit (LOD) of the MIP-based devices was 0.7 ng/mL , assuming three times the standard deviation of the blank response. In SWV (Figure 4D), a similar behaviour to that observed in the EIS assays was present. The average

slope was of $-2.3 \mu\text{A}/\text{decade} \cdot (\mu\text{g}/\text{mL})^{-1}$ (data were obtained again converting the slope current ratio of Figure 4D into current units) with a same linear range to that in EIS, 0.01 $\mu\text{g}/\text{mL}$ up to 60 $\mu\text{g}/\text{mL}$ (Figure 4F). The LOD in this case was 0.9 ng/mL which is also very close to the EIS LOD.

—Please insert Figure 4 here

The response of NIP-based devices is lower than the corresponding MIP ones, but we can observe some non-specific binding response at high target concentrations. This response (which can be observed in Figure 4B) is probably due to protein-protein and/or polymer-protein interactions (π - π or hydrophobic interactions). MIPs also suffer from a certain degree of non-specific binding, and the MIP- R_{ct} value is higher (Figure 4A) than the R_{ct} value corresponding to the saturated level reached during the process of fabrication (Figure 3A).

The precision of the analytical devices in the EIS and SWV assays was assessed via the standard deviation of the collected data, considering three different assays with three different devices, taken on different days. The corresponding standard deviations are expressed as error bars in the corresponding calibration curves, shown in Figures 4C and 4F. Interestingly, SWV showed more precise data than EIS. Since SWV was also more rapid than the EIS assays (because SWV measurements took ~ 5 s, while EIS measurements were ~ 7 min), this technique was chosen for further analysis with the home-made (HP C-PE) electrodes.

3.5 Binding isotherm

The artificial receptors described herein were further evaluated in terms of affinity toward their target analyte with the aim of monitoring the strength of the FFPM binding to its rebinding

position on the artificially-generated polymeric site. This was done by monitoring the analytical data produced by incubating the rebinding sites on the MIP film with different concentrations of FFPM and recording the differences generated in terms of their analytical signal. These data were further used to calculate an apparent dissociation constant (K_D) and the maximum binding of the target (ΔR_{ct}^{max} or ΔI^{max}). K_D is the indication of the concentration of FFPM at half of the maximum response. If K_D is a low value, a large binding affinity is present as the reaction approached the maximum response more rapidly, while a high K_D value indicates that the sensor does not efficiently bind to FFPM.

Globally speaking, the Langmuir isotherm model is used to study the binding affinity of the substrate with a homogenous test sample. Herein a heterogeneous sample (i.e. flagellar filaments of different lengths) was used to observe the binding affinity with the surface of the artificial receptors by assuming a simplification of the Langmuir isotherm model.

The isotherm analysis of a typical antibody/antigen behaviour generates the hyperbolic response [32] shown in [Figure S5](#) (Supplementary Information), for both EIS and SWV data. Also, changes in K_D are sensitive to variations in protein access/binding [36,37] and can be interpreted here in terms of barriers to antigen-artificial receptor access.

In EIS ([Figure S5A](#)), the MIP-based sensors presented ΔR_{ct}^{max} and K_D of $\sim 9.7 \text{ k}\Omega/\text{cm}^2$ and $0.5 \text{ }\mu\text{g/mL}$ respectively. The R_{ct} and $R_{O_{ct}}$ indicated the normalized and baseline charge transfer resistance values of the sensor respectively, and thus the signal density (ΔR_{ct} per unit area of electrode, where $\Delta R_{ct} = (R_{ct} - R_{O_{ct}})$) represented the binding adsorption for each concentration of FFPM. The signal density of the MIP films increased after each addition of FFPM (until saturation). In contrast, the NIP films had no significant signal variation throughout the FFPM addition, showing no or random affinity toward the protein.

In SWV ([Figure S5B](#)), the MIP-based sensors presented maximum binding (ΔI^{max}) of $\sim 23.4 \text{ }\mu\text{A}/\text{cm}^2$ with a dissociation constant of K_D $0.4 \text{ }\mu\text{g/mL}$. I and I_o indicated the normalized and

baseline currents respectively. The plot of signal density ($-ΔI$ per unit area of electrode, where $-ΔI = (I - I_0)$) versus FFPM concentration again showed that the MIPs were highly sensitive to FFPM, whereas the NIPs were rather insensitive. Interestingly, the results of SWV are closely related to the EIS-based results.

Overall, NIPs displayed almost negligible affinity toward FFPM compared to the MIP-based sensors. This showed a predictable and sensitive response of the MIPs against FFPM concentration, since the differences between NIPs and MIPs were only the absence or presence of FFPM-tailored binding sites at the receptor surface.

3.6 Selectivity

The selectivity of the sensor was evaluated by EIS and SWV measurements (Figure 5) using the competitive assay [28], in which the target FFPM was allowed to compete for the same surface with a foreign element that is expected to behave as an interfering species. The assay was done by setting the FFPM concentration to 1 $\mu\text{g/mL}$; the solutions of the interfering species were globular proteins (BSA 0.85 $\mu\text{g/mL}$, PA 0.51 $\mu\text{g/mL}$) and flagellar filaments from two different bacterial species (FFED 1.03 $\mu\text{g/mL}$, FFAA 1.27 $\mu\text{g/mL}$).

The response of the MIP-based sensors was checked using solutions with only FFPM or FFPM plus the interfering species. The time and conditions were set as in the calibration of the sensors.

—Please insert Figure 5 here

The average percentage of deviation produced by each interfering species in the pure FFPM solution was 1.9% for BSA, 7.8% for PA, -5.7% for FFED and 0.9% for FFAA in EIS studies, and 2.4% for BSA, 3.3% for PA, -3.9% for FFED and 1.9% for FFAA in SWV evaluations.

The typical EIS-based spectra and SWV voltammograms obtained herein can be seen in [Figures 5A and 5B](#) respectively.

Overall, negligible interference was found from the competing proteins (BSA, PA, FFED and FFAA), with changes in current and/or charge transfer resistance always below 10% in the $\mu\text{g/mL}$ protein level. Furthermore, and in agreement with the previous precision data, the sensors displayed better performance in terms of selectivity when evaluated by SWV.

3.7 Application to real samples

As this research was intended for field water monitoring and low-cost applications, the possibility of using the home-made paper-based devices (HP C-PE) in this context was tested. Tap water was used as a sample with the aim of assessing possible application to the proposed devices and tested as proof of concept for the detection of FFPM. The results obtained are presented in [Figure 6](#).

—Please insert Figure 6 here

In the absence of actual contaminated water, the tap water was spiked and diluted four times in MES buffer due to the need to add standards. The resulting solutions were monitored, as in a calibration where the background was a real water sample artificially contaminated. In general, the obtained results indicated good features in terms of concentration range of linear response ($0.01 \mu\text{g/mL}$ to $100 \mu\text{g/mL}$), LOD (0.6 ng/mL) and slope ($-0.40 \mu\text{A/decade} \cdot (\mu\text{g/mL})^{-1}$, with the slope being obtained by again converting the slope current ratio of [Figure 6B](#) to current units). Comparing these results with the FFPM calibration curve in MES buffer pH 5.0, the LOD is of the same order magnitude.

The most interesting information to come out of this experiment is that the home-made disposable device (HP C-PE) showed sensing performance for detecting FFPM from tap water with very similar analytical parameters to those obtained using SWCNTs-SPE in MES buffer, which would be a great advance toward making home-made easy-tailored electrodes that are cost-effective and portable bio-sensing devices.

4. Conclusions

In this paper an artificial receptor based on molecular imprinting for the direct electrochemical detection of bacterial flagellar filaments is presented for the first time. The non-imprinted devices showed random binding, making this sensor especially suitable for the detection of bacterial surface proteins. In addition, and to the best of our knowledge, the home-made device (HP C-PE) is the first home-made paper-based approach for making electrochemically-based artificial protein receptors, which would be a cost-effective portable device and a useful tool in the field of electrochemical research and diagnostic in developing countries.

Flagellar filaments are located on the outer surface of bacteria and can act as markers for detecting and/or identifying bacteria. In this regard, clinical studies have revealed the significant role of flagellar filaments in the characterization and affiliation of anaerobic bacteria [16]. The device displays good precision, high selectivity, a low detection limit, cost-effectiveness, and also offers the advantages of disposability and portability, simple instrumentation and easy preparation for the detection of flagellar filaments of *P. mirabilis*. Flagellar filaments can act as markers for detecting and/or identifying bacteria, and this work

can be seen as one of the initial steps for detecting bacteria using molecularly imprinted polymer-based devices.

Acknowledgments

The Catalan Government and the European Research Council are acknowledged for the financial support of MARK PhD Fellowship (2013FI_B00842) and Starting Grant, 3P's, GA 311086 respectively. The URV team would also like to thank the Spanish Ministerio de Economía y Competitividad for its financial support (Project CTQ2010-18717).

References

- [1] S. Merkl, D. Vornicescu, N. Dassinger, M. Keusgen, Detection of whole cells using reflectometric interference spectroscopy, *Phys. Status Solidi A*. 1422 (2014) 1416–1422.
- [2] E. Heyduk, T. Heyduk, Fluorescent homogeneous immunosensors for detecting pathogenic bacteria, *Anal. Biochem.* 396 (2010) 298–303.
- [3] X. Guo, C. Lin, S. Chen, R. Ye, V.C.H. Wu, A piezoelectric immunosensor for specific capture and enrichment of viable pathogens by quartz crystal microbalance sensor, followed by detection with antibody-functionalized gold nanoparticles, *Biosens. Bioelectron.* 38 (2012) 177–183.
- [4] N. Wangmaung, S. Chomean, C. Promptmas, S. Mas-oodi, Silver quartz crystal microbalance for differential diagnosis of plasmodium falciparum and plasmodium vivax in single and mixed infection, *Biosens. Bioelectron.* 62 (2014) 295–301.
- [5] L. Lu, G. Chee, K. Yamada, S. Jun, Electrochemical impedance spectroscopic technique with a functionalized microwire sensor for rapid detection of foodborne pathogens, *Biosens. Bioelectron.* 42 (2013) 492–495.
- [6] R. Maalouf, C. Fournier-wirth, J. Coste, H. Chebib, Y. Sai, O. Vittori, et al., Label-free detection of bacteria by electrochemical impedance spectroscopy: comparison to surface plasmon resonance, *Anal. Chem.* 79 (2007) 4879–4886.
- [7] C. Sporer, V. Teixeira, Highly sensitive detection of pathogen Escherichia coli O157 : H7 by electrochemical impedance spectroscopy, *Biosens. Bioelectron.* 45 (2013) 174–180.
- [8] G.A. Zelada-Guillen, J. Riu, A. Düzgün, F.X. Rius, Immediate detection of living bacteria at ultralow concentrations using a carbon nanotube based potentiometric aptasensor, *Angew. Chem. Int. Ed.* 48 (2009) 7334–7337.
- [9] M.A. Nadkarni, F.E. Martin, N.A. Jacques, N. Hunter, Determination of bacterial load by real-time PCR using a broad-range (universal) probe and primers set, *Microbiology.* 148 (2002) 257–266.
- [10] L. Yang, C. Ruan, Y. Li, Detection of viable Salmonella typhimurium by impedance measurement of electrode capacitance and medium resistance, *Biosens. Bioelectron.* 19 (2003) 495–502.
- [11] L. Yang, R. Bashir, Electrical/electrochemical impedance for rapid detection of foodborne pathogenic bacteria, *Biotechnol. Adv.* 26 (2008) 135–150.
- [12] E.A. Barlaan, M. Sugimori, S. Furukawa, K. Takeuchi, Electronic microarray analysis of 16S rDNA amplicons for bacterial detection, *J. Biotechnol.* 115 (2005) 11–21.
- [13] M. Ikeda, N. Yamaguchi, K. Tani, M. Nasu, Detection of food poisoning bacteria in fresh vegetables using DNA microarray, *J. Heal. Sci.* 52 (2006) 36–42.
- [14] J.R. Uzarski, C.M. Mello, Detection and classification of related lipopolysaccharides via a small array of immobilized antimicrobial peptides, *Anal. Chem.* 84 (2012) 7359–7366.
- [15] S.L. Jordana, M.D.L. Oliveira, C.P. De Melo, C.A.S. Andrade, Impedimetric sensor of bacterial toxins based on mixed (concanavalin A)/ polyaniline films, *Colloids Surfaces B Biointerfaces.* 117 (2014) 549–554.
- [16] H. Kodaka, A.Y. Armfield, G.L. Lombard, V.R. Dowell, J R. et al, Practical procedure

- for demonstrating bacterial flagella, *J. Clin. Microbiol.* 16 (1982) 948–952.
- [17] C. Winstanley, J.A.W. Morgan, The bacterial flagellin gene as a biomarker for detection, population genetics and epidemiological analysis, *Microbiology*. 143 (1997) 3071–3084.
- [18] H. Grossart, L. Riemann, F. Azam, Bacterial motility in the sea and its ecological implications, *Aquat Microbial Ecol.* 25 (2001) 247–258.
- [19] Clark W. A., A simplified leifson flagella stain, *J. Clin. Microbiol.* 3 (1976) 632–634.
- [20] L. Forbes, Rapid flagella stain, *J. Clin. Microbiol.* 13 (1981) 807–809.
- [21] Y. Wang, Z. Ye, Y. Ying, New trends in impedimetric biosensors for the detection of foodborne pathogenic bacteria, *Sensors*. 12 (2012) 3449–3471.
- [22] M.J. Whitcombe, I. Chianella, L. Larcombe, S.A. Piletsky, J. Noble, A. Horgan, The rational development of molecularly imprinted polymer-based sensors for protein detection, *Chem. Soc. Rev.* 40 (2011) 1547–1571. doi:10.1039/c0cs00049c.
- [23] J. Liu, Q. Deng, D. Tao, K. Yang, L. Zhang, Z. Liang, et al., Preparation of protein imprinted materials by hierarchical imprinting techniques and application in selective depletion of albumin from human serum, *Sci. Rep.* 4:5487 (2014) 1–6.
- [24] E. Verheyen, J.P. Schillemans, M. Van Wijk, M.-A. Demeniex, W.E. Hennink, C.F. Van Nostrum, Challenges for the effective molecular imprinting of proteins, *Biomaterials*. 32 (2011) 3008–3020.
- [25] K. Haupt, Imprinted polymers —Tailor-made mimics of antibodies and receptors, *Chem. Commun.* (2003) 171–178.
- [26] S. Lingxin, As featured in: molecular imprinting: perspectives and applications, *Chem. Soc. Rev.* 45 (2016) 2137–2211.
- [27] F.K. Bahrani, D.E. Johnson, D. Robbins, H.L.T. Mobley, *Proteus mirabilis* flagella and MR/P fimbriae: isolation, purification, N-terminal analysis, and serum antibody response following experimental urinary tract infection, *Infect. Immun.* 59 (1991) 3574–3580.
- [28] F.T.C. Moreira, S. Sharma, R.A.F. Dutra, J.P.C. Noronha, A.E.G. Cass, M.G.F. Sales, Smart plastic antibody material (SPAM) tailored on disposable screen printed electrodes for protein recognition: application to myoglobin detection, *Biosens. Bioelectron.* 45 (2013) 237–244.
- [29] M.A. Panagopoulou, D. V Stergiou, I.G. Roussis, M.I. Prodromidis, Impedimetric biosensor for the assessment of the clotting activity of rennet, *Anal. Chem.* 82 (2010) 8629–8636.
- [30] I.I. Suni, Impedance methods for electrochemical sensors using nanomaterials, *TrAC - Trends Anal. Chem.* 27 (2008) 604–611.
- [31] J.S. Daniels, Label-free impedance biosensors: opportunities and challenges, *Electroanalysis*. 19 (2008) 1239–1257.
- [32] S.J. Ding, B.W. Chang, C.C. Wu, M.F. Lai, H.C. Chang, Electrochemical evaluation of avidin-biotin interaction on self-assembled gold electrodes, *Electrochim. Acta.* 50 (2005) 3660–3666.
- [33] S.J. Ding, B.W. Chang, C.C. Wu, M.F. Lai, H.C. Chang, Impedance spectral studies of self-assembly of alkanethiols with different chain lengths using different immobilization strategies on Au electrodes, *Anal. Chim. Acta.* 554 (2005) 43–51.

- [34] M. Yuqing, C. Jianrong, W. Xiaohua, Using electropolymerized non-conducting polymers to develop enzyme amperometric biosensors, *Trends Biotechnol.* 22 (2004) 227–231.
- [35] Y. Samet, D. Kraiem, R. Abdelhedi, Electropolymerization of phenol, o-nitrophenol and o-methoxyphenol on gold and carbon steel materials and their corrosion protection effects, *Prog. Org. Coatings.* 69 (2010) 335–343.
- [36] S. V Sasso, R.J. Pierce, R. Walla, A.M. Yacynych, Electropolymerized 1,2-diaminobenzene as a means to prevent interferences and fouling and to stabilize immobilized enzyme in electrochemical biosensors, *Anal. Chem.* 62 (1990) 1111–1117.
- [37] S.A. Rothwell, S.J. Killoran, R.D. O'Neill, Enzyme immobilization strategies and electropolymerization conditions to control sensitivity and selectivity parameters of a polymer-enzyme composite glucose biosensor, *Sensors.* 10 (2010) 6439–6462.

Legends for Figures

Figure 1 Schematic presentation of MIP synthesis: (A) *P. mirabilis* with flagellar filaments, (B) Flagellar filaments (FFPM) removed from the cells by shearing in a vortex with a glass bar and then passing repetitively through a syringe, (C) Immobilized FFPM at the working area of SWCNTs-SPE / HP C-PE, (D) Imprinting stage after electropolymerization of phenol in acetate buffer, (E) Binding sites formation after template removal by proteinase K.

Figure 2 CV data for the (A) electrochemical synthesis of MIP and NIP films at SWCNTs-SPEs (15 CV cycles) and (B) the electrical response of the thus-obtained films in a standard iron redox probe of 5.0 mM $[\text{Fe}(\text{CN})_6]^{3-}$ and 5.0 mM $[\text{Fe}(\text{CN})_6]^{4-}$, in MES buffer pH 5.0. CV data for the (C) electrochemical synthesis of MIP and NIP films at HP C-PEs (15 CV cycles) and (D) the electrical response of the thus-obtained films in a standard iron redox probe of 5.0 mM $[\text{Fe}(\text{CN})_6]^{3-}$ and 5.0 mM $[\text{Fe}(\text{CN})_6]^{4-}$, in MES buffer pH 5.0.

Figure 3 Follow-up of the protein template exit from the polymeric material using EIS and SWV. Data from the clean SWCNTs-SPE, after polymerization and after template removal. (A) EIS data for MIPs (B) EIS data for NIPs (C) SWV data for MIPs (D) SWV data for NIPs. The redox probes were 5.0 mM $[\text{Fe}(\text{CN})_6]^{3-}$ and 5.0 mM $[\text{Fe}(\text{CN})_6]^{4-}$ solution, prepared in MES buffer pH 5.0.

Figure 4 EIS (A, B and C) and SWV (D, E and F) measurements of (A, D) MIP and (B, E) NIP-based devices upon increasing FFPM concentrations. The calibration curves for EIS data (MIP and NIP devices) are shown in C, and the calibration curves for SWV data (MIP and NIP devices) are shown in F. The error bars in the calibration lines in C and F correspond to 3 measurements from three independent devices. The redox

probes were 5.0 mM $[\text{Fe}(\text{CN})_6]^{3-}$ and 5.0 mM $[\text{Fe}(\text{CN})_6]^{4-}$, prepared in MES buffer, pH 5.0.

Figure 5 Selectivity study with (A) EIS and corresponding bar diagram (the percentage corresponds to the deviation in the response caused by the interference) in (B); and with (C) SWV and corresponding bar diagram (the percentage corresponds to the response caused by the interference) in (D).

Figure 6 SWV based measurements (A) of MIP-based HP C-PE and the corresponding calibration curve (B) in 5.0 mM $[\text{Fe}(\text{CN})_6]^{3-}$ and 5.0 mM $[\text{Fe}(\text{CN})_6]^{4-}$ by spiking FFPM in tap water within 0.01 $\mu\text{g}/\text{mL}$ and 100 $\mu\text{g}/\text{mL}$.

Figure 1

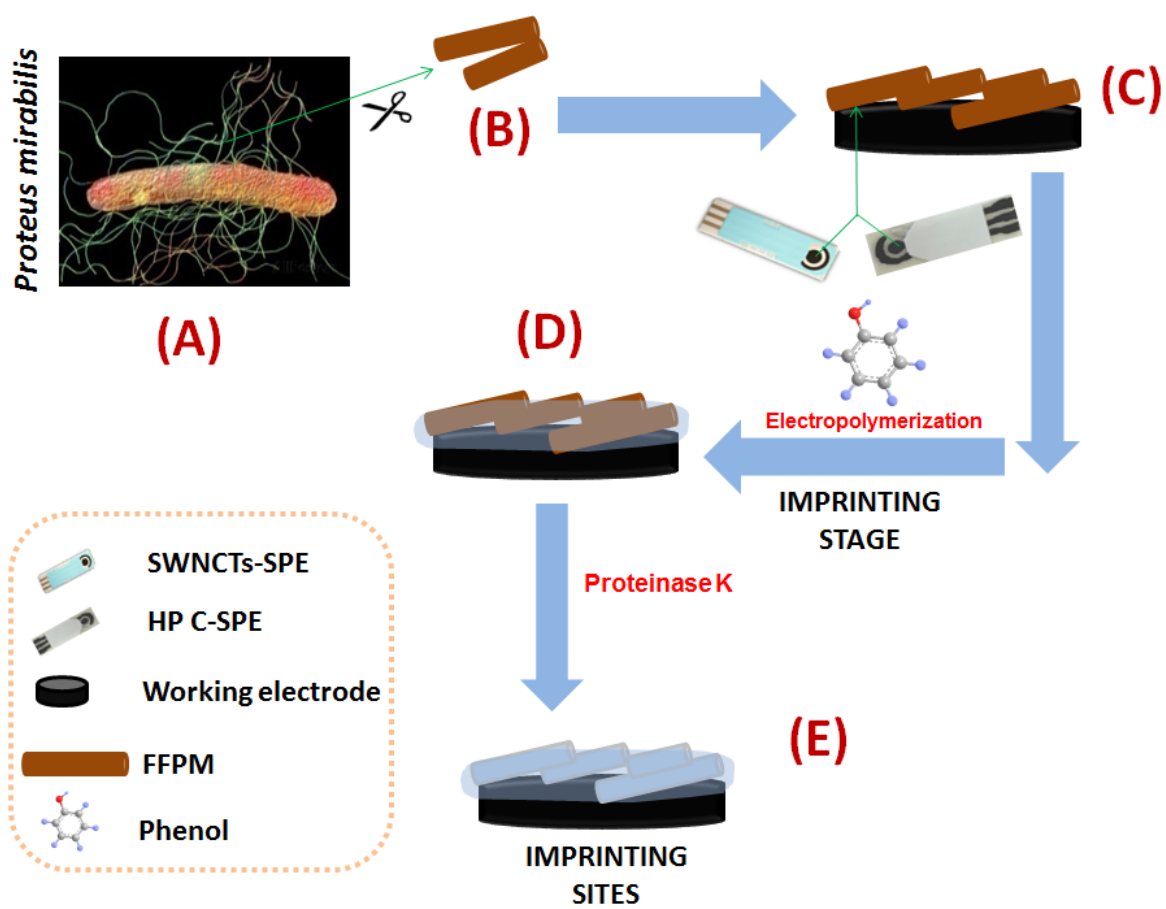


Figure 2

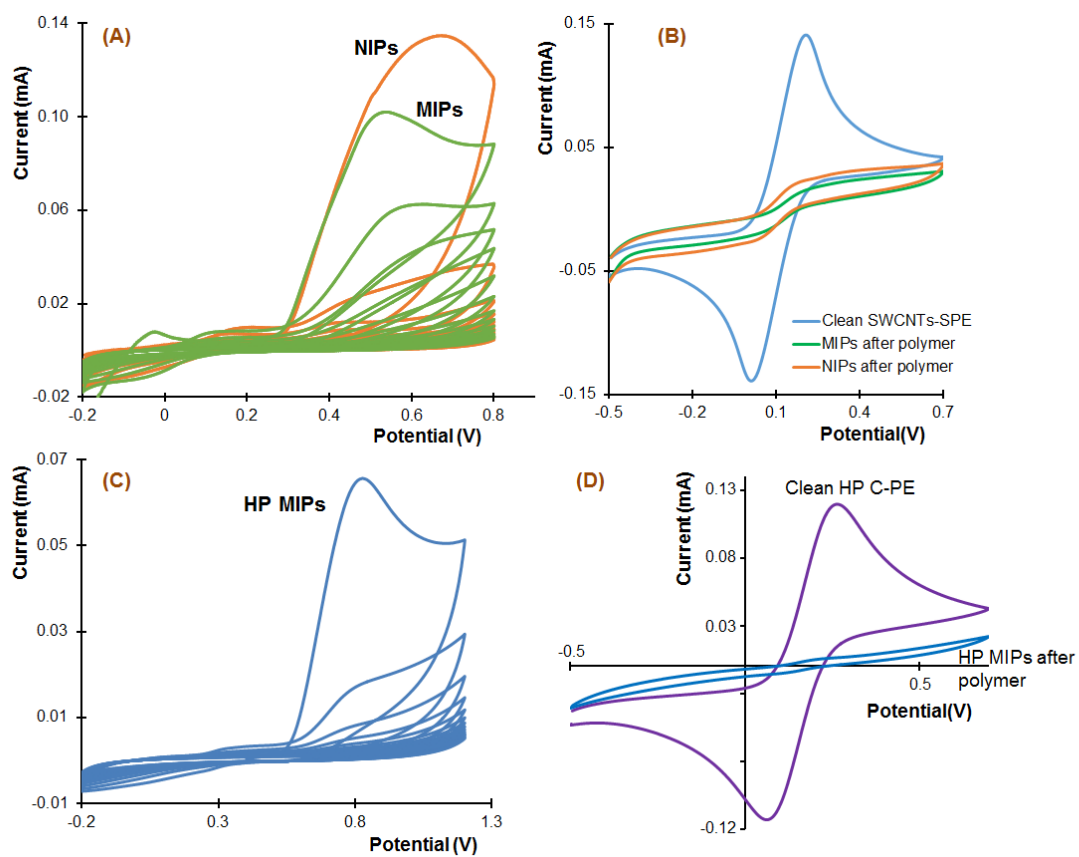


Figure 3

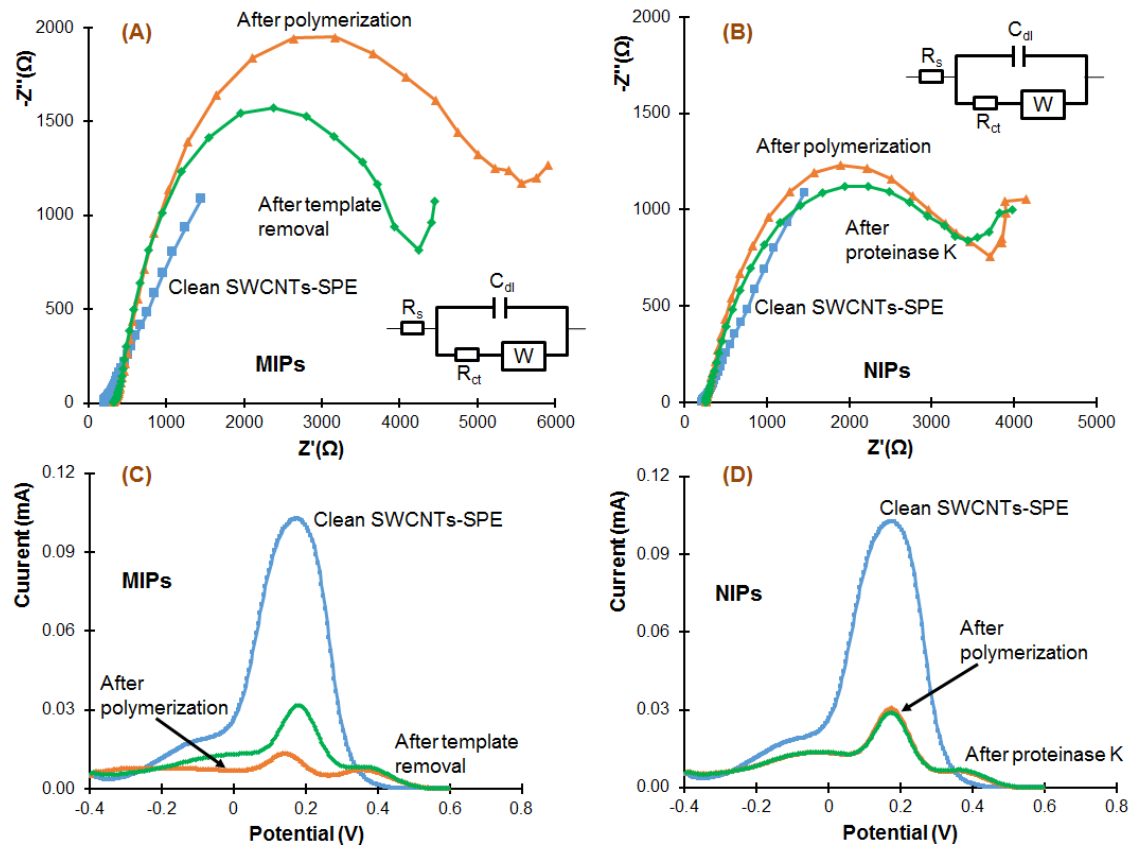


Figure 4

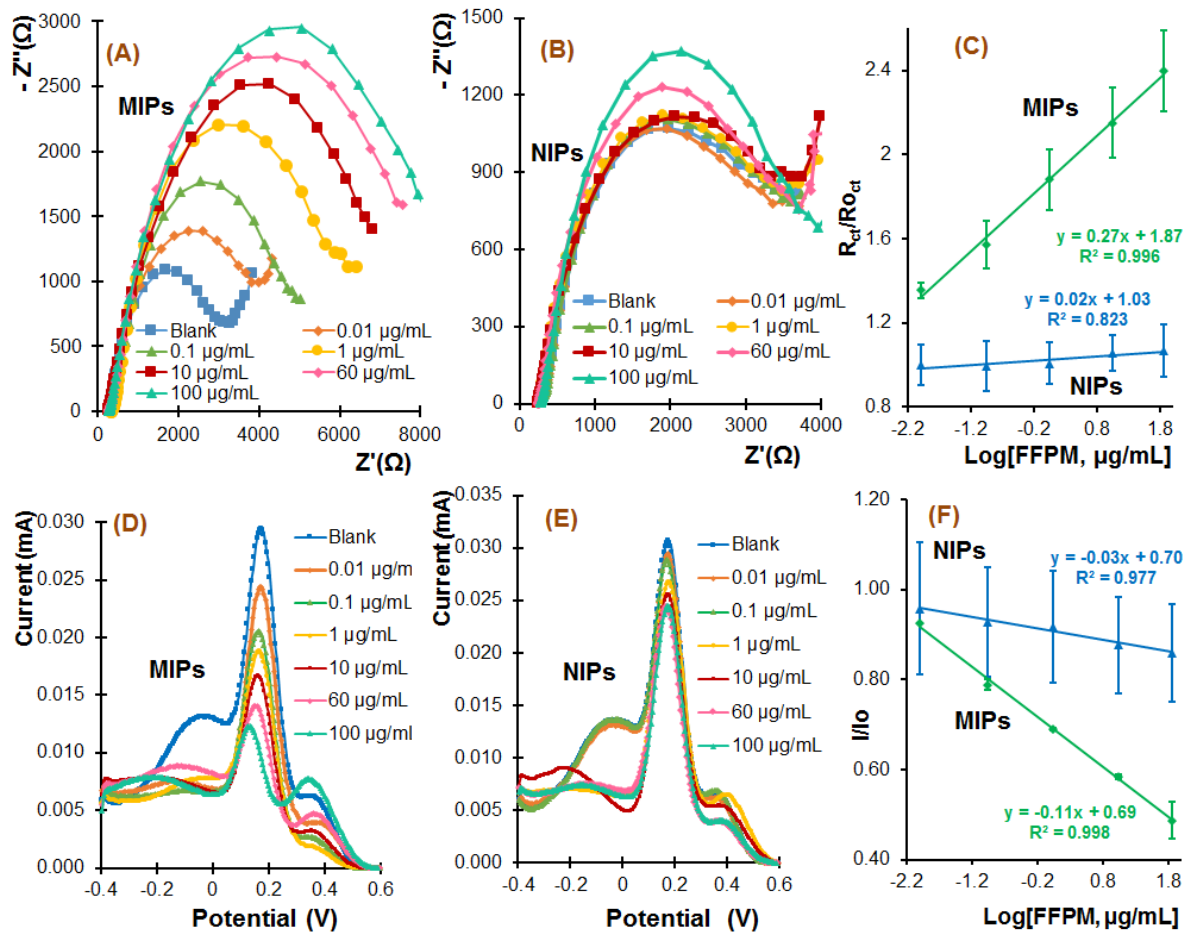


Figure 5

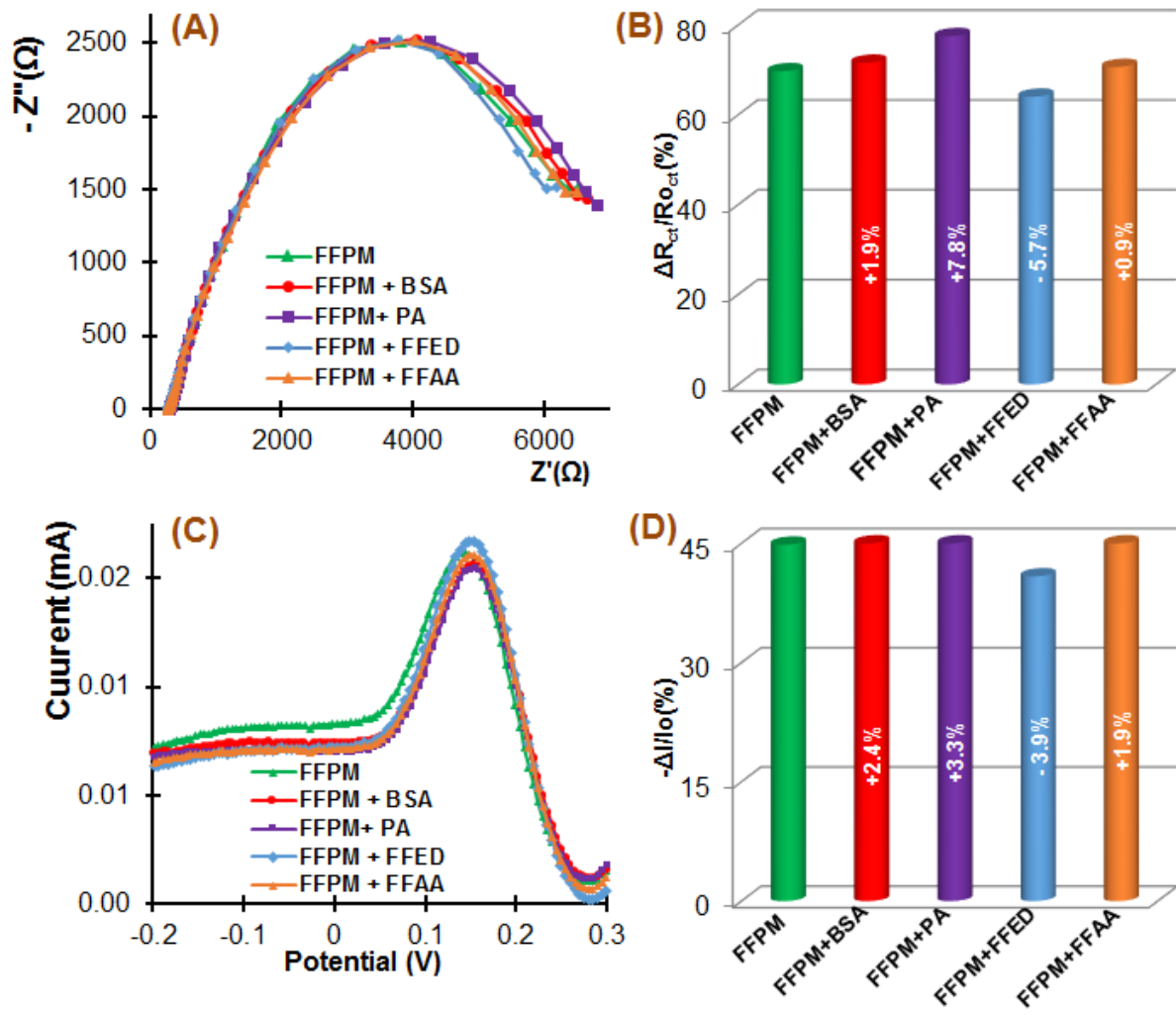


Figure 6

